

1 **The role of Ekman currents, geostrophy and Stokes**
2 **drift in the accumulation of floating microplastic**

3 **Victor Onink¹, David Wichmann^{1,2}, Philippe Delandmeter¹, Erik van Sebille¹**

4 ¹Institute for Marine and Atmospheric Research, Utrecht University, Utrecht, the Netherlands.

5 ²Centre for Complex Systems Studies, Utrecht University, Utrecht, the Netherlands.

6 **Key Points:**

- 7 • Modeled microplastic distributions agree with observed distributions in the North
8 Pacific and North Atlantic
9 • Ekman currents are the main process behind microplastic accumulation in the sub-
10 tropical ocean gyres
11 • Stokes drift contributes to microplastic transport to the polar regions

Corresponding author: Victor Onink, v.onink@uu.nl

Abstract

Floating microplastic in the oceans is known to accumulate in the subtropical ocean gyres, but unclear is still what causes that accumulation. We investigate the role of various physical processes, such as surface Ekman and geostrophic currents, surface Stokes drift and mesoscale eddy activity, on the global surface distribution of floating microplastic with Lagrangian particle tracking using GlobCurrent and WaveWatch III reanalysis products. Globally, we find that the locations of the garbage patches are largely determined by the Ekman currents. Separate simulations of the North Pacific and North Atlantic show that the locations of the modeled garbage patches using GlobCurrent Total (Ekman + geostrophic) currents agree with observed microplastic distributions. Geostrophic currents and Stokes drift do not contribute to garbage patch formation in the subtropics, but Stokes drift leads to increased microplastic transport to the polar regions. Transport due to Stokes drift is found to be more sensitive to the temporal resolution of the dataset than the other current components. Since the WaveWatch III Stokes drift and GlobCurrent Ekman current datasets are not independent, combining Stokes drift with the other current components leads to an overestimation of the effects of Stokes drift and there is therefore a need for independent measurements of the different ocean circulation components. In the North Pacific, we find that microplastic tends to accumulate in regions of relatively low eddy kinetic energy, indicating low mesoscale eddy activity, but we do not see similar trends in the North Atlantic.

Plain Language Summary

Microplastic is a common form of pollution in the oceans, and high floating microplastic concentrations tend to be observed at the surface in the subtropical ocean gyres. These regions are commonly referred to as garbage patches. However, the physical processes that control the buildup in these regions are not yet fully understood. Therefore, we model microplastic transport with various surface current component that correspond to different physical processes. We do this with Lagrangian modeling, where microplastic is represented by virtual particles that are transported by ocean currents. We found good agreement between the modeled distribution with the full surface currents with observations in the North Pacific and North Atlantic and find that the microplastic accumulation is mainly due to the wind-driven Ekman currents. Meanwhile, wave-driven Stokes drift results in microplastic transport to the polar regions. Since Stokes drift has not consistently been included in microplastic transport modeling, microplastic contamination of the polar regions might be more severe than currently expected.

1 Introduction

The surface ocean circulation is driven by a large number of processes and is traditionally decomposed into various current components. These include the wind-driven Ekman currents, the geostrophic currents, and wave-induced Stokes drift. It has been shown that the Ekman and geostrophic currents play different roles in marine debris accumulation (Kubota, 1994; Kubota, Takayama, & Namimoto, 2005; Martinez, Maamaatuaiahutapu, & Taillandier, 2009), while Stokes drift has been shown to be important for kelp (Fraser et al., 2018) and oil (Drivdal, Broström, & Christensen, 2014) transport. However, the contribution of Stokes drift using reanalysis data to transport of floating plastic debris has not been studied.

Plastic debris has been found in a large number of marine habitats, such as in the open ocean (Cózar et al., 2014, 2017; Eriksen et al., 2014, 2013; Lebreton et al., 2018), on coastlines (Pieper, Ventura, Martins, & Cunha, 2015; Thompson et al., 2004; Young & Elliott, 2016) and on the sea floor (Galgani et al., 2000; Van Cauwenberghe, Vanreusel, Mees, & Janssen, 2013). The majority of plastic debris found at sea is non-biodegradable (Duhec, Jeanne, Maximenko, & Hafner, 2015; Morét-Ferguson et al., 2010) and can per-

62 sist for decades in the open ocean (Lebreton et al., 2018), where it can cause harm to
63 marine life through ingestion (Mascarenhas, Santos, & Zeppelini, 2004; van Franeker &
64 Law, 2015), entanglement (Henderson, 2001) and by acting as a potential pathway for
65 habitat invasion by alien species (Molnar, Gamboa, Revenga, & Spalding, 2008).

66 An estimated 4.8 - 12.7 million tons of plastic entered the ocean in 2010 (Jambeck
67 et al., 2015), and buoyant plastic debris is known to accumulate in the subtropical ocean
68 gyres in each of the ocean basins (Cózar et al., 2014; Eriksen et al., 2014; Law et al., 2010,
69 2014). For the Pacific basins, this accumulation has been found to be caused by surface
70 Ekman currents (Kubota, 1994; Kubota et al., 2005; Martinez et al., 2009). The geostrophic
71 currents contribute to debris transport, but due to their non-divergent nature do not lead
72 to debris accumulation on their own Martinez et al. (2009). Kubota (1994) found that
73 Stokes drift does not significantly contribute to debris transport, but parametrized Stokes
74 drift as windage with climatological mean wind fields and as such did not take ocean swell
75 into account, which is not locally generated. Windage represents the force of surface wind
76 on exposed portions of an object above the ocean surface and windage effects have been
77 found to have a significant impact on the trajectories of large objects (Trinanes et al.,
78 2016). For microplastic, windage can play a significant role with low-density plastic such
79 as polystyrene, but for higher density plastics the microplastic particles would be largely
80 below the surface and thus not be exposed to much direct wind stress (Chubarenko, Bagaev,
81 Zobkov, & Esiukova, 2016).

82 Comparisons of modeled microplastic distributions with observed microplastic con-
83 centrations were done by van Sebille et al. (2015), who modeled the global distribution
84 of microplastic based either on drogued surface drifter trajectories (Maximenko, Hafner,
85 & Niiler, 2012; van Sebille, England, & Froyland, 2012) or using HYCOM/NCODA sur-
86 face currents (Lebreton, Greer, & Borrero, 2012) and compared the distributions with
87 observations from surface-trawling plankton nets. It was found that the modeled distri-
88 butions in the North Pacific closely correlate to spatial patterns in the observations, but
89 that in the North Atlantic the agreement of the modeled distributions with observations
90 is weaker. None of the models completely accounted for Stokes drift, which might there-
91 fore be a possible explanation for the observed discrepancies.

92 Processes that act on scales smaller than the mesoscale also play a role in microplastic
93 accumulation. Martinez et al. (2009) found a tendency for debris in the South Pa-
94 cific to accumulate in regions of relatively low eddy kinetic energy (EKE), which can be
95 considered as a proxy for mesoscale eddy activity (Eden & Böning, 2002). Microplas-
96 tic concentrations in an anticyclonic eddy have been found to be more than nine times
97 higher than in a cyclonic eddy (Brach et al., 2018), while resolving mesoscale eddies in-
98 creases the ability of microplastic to leave garbage patches in debris simulations (Maes,
99 Blanke, & Martinez, 2016). However, the link between mesoscale eddy activity and plas-
100 tic debris accumulation in the North Pacific and North Atlantic has not been considered
101 so far.

102 Since different components of the the ocean circulations can change on different time
103 scales, the temporal resolution of ocean circulation datasets can impact modeled trans-
104 port. Maximenko et al. (2012) reported that temporal variability of the ocean currents
105 has a strong influence of debris transport, as particles do not follow mean ocean current
106 streamlines to reach debris accumulation regions. Particularly transport due to Stokes
107 drift is dependent on the temporal resolution of the dataset, since Stokes drift is depen-
108 dent on the wave field, which can change on very short time scales by changes in local
109 weather conditions (Bennett & Mulligan, 2017; Montiel, Squire, Doble, Thomson, & Wad-
110 hams, 2018).

111 In this paper we study the contributions of the Ekman and geostrophic currents
112 and Stokes drift on the location of microplastic accumulation regions (henceforth referred
113 to as garbage patches) on a global scale, with particular focus on the North Pacific and

114 the North Atlantic. This is done by means of Lagrangian simulations with ocean circu-
 115 lation data from reanalysis products (Rio, Johannessen, & Donlan, 2016; Tolman, 2009)
 116 including surface Ekman and geostrophic currents and surface Stokes drift. The recently
 117 proposed Sea surface KInematics Multiscale (SKIM) monitoring satellite (Ardhuin et al.,
 118 2018) would be able to measure ocean surface transport components such as Stokes drift
 119 directly. Therefore, the role of Stokes drift is of particular interest seeing how its effect
 120 on the transport of plastic debris has not been extensively considered (van den Bremer
 121 & Breivik, 2018). We also consider how transport is dependent on the temporal reso-
 122 lution of the datasets. Since windage has been used as a proxy for Stokes drift in the past
 123 Breivik and Allen (2008); Kubota (1994), we compare the transport due to Stokes drift
 124 from the WaveWatch III hindcast Tolman (2009) with various windage scenarios to in-
 125 vestigate whether windage adequately captures Stokes drift dynamics. The modeled mi-
 126 croplastic distributions in the North Pacific and North Atlantic are compared with ob-
 127 served microplastic concentrations measured with surface-trawling plankton nets from
 128 the dataset compiled by van Sebille et al. (2015). Finally, we examine the link between
 129 mesoscale eddy activity and microplastic accumulation.

130 2 Materials and Methods

131 2.1 Ocean Surface Current Datasets

132 We use several different reanalysis surface current data sets outlined in Table 1 for
 133 the period of 2002-2014. The Ekman and Geostrophic flow fields are from the GlobCur-
 134 rent project (Rio et al., 2016), which combines satellite observations and in-situ mea-
 135 surements to obtain estimates of the surface circulation. Rio et al. (2016) make an ini-
 136 tial estimate of the Geostrophic currents from altimeter maps and subtract this from sur-
 137 face velocities of ARGO floats to get an estimate of the non-geostrophic velocity of each
 138 drifter, which is referred to as the surface Ekman velocity. The Ekman velocities $\vec{u}_{ek}(z)$
 139 are parametrized by Rio et al. (2016) with an amplification factor $\beta(z)$ and Ekman ve-
 140 locity angle $\theta(z)$ by applying a least squares fit between measured Ekman velocities from
 141 ARGO drifters and surface wind stress $\vec{\tau}$ data from ERA-Interim (Dee et al., 2011). Based
 142 on 841,746 ARGO drifter Ekman velocities, the surface Ekman currents are found by
 143 Rio et al. (2016) to be at an angle of $\theta(0) = 30.75^\circ$ to the wind stress (to the right in
 144 the Northern Hemisphere, to the left in the Southern Hemisphere), with an amplifica-
 145 tion factor of $\beta(0) = 0.61 \text{ m}^2 \text{ s kg}^{-1}$. Using 15m-drogued drifters from the Surface Ve-
 146 locity Program (SVP), the Ekman current parameters at 15m depth are $\theta(15\text{m}) = 48.18^\circ$
 147 and $\beta(15\text{m}) = 0.25 \text{ m}^2 \text{ s kg}^{-1}$.

148 The Geostrophic velocities of 15m-drogued and undrogued surface drifters from the
 149 Surface Velocity Program (SVP) are found by subtracting the Ekman velocities from the
 150 drifter velocities. Rio et al. (2016) uses the measured Geostrophic velocities to update
 151 the initial geodetic mean dynamic topography (MDT) to determine the CNES-CLS13
 152 MDT from which the final Geostrophic velocities are computed. This incorporation of
 153 in-situ observations provides missing short-scale information for the boundary currents
 154 and equatorial regions that would be missing with just a geodetic approach (Rio, Mulet,
 155 & Picot, 2014). The Total surface currents are the sum of the surface Geostrophic ve-
 156 locities and the surface Ekman velocities.

157 The surface Stokes drift is from the WaveWatch III hindcast dataset (Tolman, 1997,
 158 2009), where the magnitude and direction of the Stokes drift is based on the wavenumber-
 159 direction spectrum (Webb & Fox-Kemper, 2015). The 2002-2014 temporal means of the
 160 GlobCurrent and WaveWatch flow fields are shown in Figure 1.

161 It must be noted that the GlobCurrent and WaveWatch III datasets are not inde-
 162 pendent. The parametrization of the GlobCurrent Ekman currents does not contain a

Table 1. Overview of the datasets used for particle advection in the simulations.

Flow Field	Dataset	Spatial Resolution	Temporal Resolution	Source
Ekman currents	GlobCurrent v3	1/4°	3 h	Rio et al. (2016)
	Ekman Hs Currents			
Geostrophic currents	GlobCurrent v3	1/4°	24 h	Rio et al. (2016)
	Geostrophic Currents			
Total currents	GlobCurrent v3	1/4°	3 h	Rio et al. (2016)
	Total Hs Currents			
Stokes drift	WaveWatch III	1/2°	3 h	Tolman (1997, 2009)
	Surface Stokes Drift			
Windage	CFSR Surface Winds	1/2°	3 h	Saha et al. (2011)

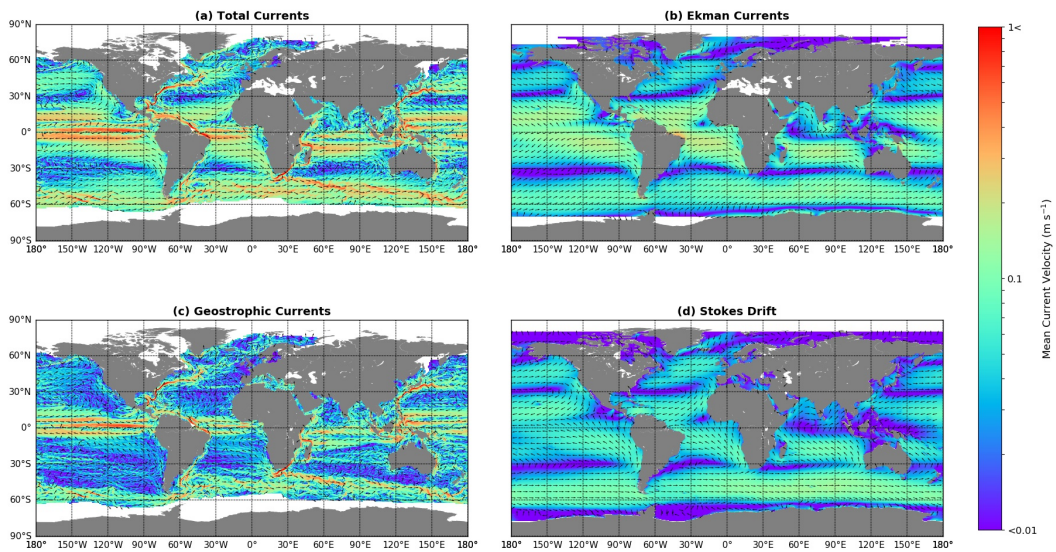


Figure 1. Temporal mean flow fields for the Total, Ekman and Geostrophic currents and the Stokes drift. Averages are taken for 2002-2014, with the normalized vectors indicating the mean direction and the colormap indicating the current magnitude. Note that the velocity scale is logarithmic.

163 correction for Stokes drift, and so summation of the flow fields will lead to an overesti-
 164 mation of the Stokes drift effect.

165 2.2 Windage Proxy

166 Windage effects are dependent on the object size, shape and buoyancy and the cou-
 167 pling strength between the local wind and the resultant windage velocity of the object
 168 is highly variable (Chubarenko et al., 2016). We use the windage classification used by
 169 Duhec et al. (2015), which classifies debris as either low windage (e.g. fishing nets and
 170 small plastic fragments), medium windage (e.g. polystyrene and partially filled PET bot-
 171 tles) or high windage (e.g. unfilled PET bottles and fishing buoys). We compare the Stokes
 172 drift with each of these windage scenarios, where the windage is 1%, 3% or 5% of the

173 local wind vector, to investigate which would be most appropriate as a proxy for Stokes
 174 drift. We use the CFSR (Saha et al., 2011) wind fields for 2002-2014 (Table 1), which
 175 is the same wind field used for the WaveWatch III hindcast (Tolman, 2009).

176 2.3 Microplastic Observation Dataset

177 The dataset of microplastic measurements taken by surface-trawling plankton nets
 178 was compiled by van Sebille et al. (2015). 11,632 trawl measurements taken between 1979
 179 and 2013 were considered by van Sebille et al. (2015), of which 6812 were collected in
 180 the North Atlantic, 2551 were collected in the North Pacific and the rest were spread out
 181 over the Southern Hemisphere and in the Mediterranean. While microplastic commonly
 182 refers to plastic debris <5 mm, van Sebille et al. (2015) refers to any plastic debris col-
 183 lected with a plankton net trawl as microplastic, as most of the plastic collected in plank-
 184 ton net trawls are small fragments. We use the same definition in all following references
 185 to microplastic.

186 Given that the samples were collected over a period of 34 years and that microplas-
 187 tic concentrations are sensitive to the vertical mixing due to surface wind stress (Kukulka,
 188 Proskurowski, Morét-Ferguson, Meyer, & Law, 2012), van Sebille et al. (2015) corrected
 189 for the sampling year and the variable wind conditions. All concentrations are ultimately
 190 expressed in terms of counts km⁻² and are binned into 1° bins. Given that the obser-
 191 vational record for the Southern Hemisphere is very limited, it is not possible to make
 192 meaningful comparisons between modeled microplastic distributions and observations
 193 for these regions. We therefore focus on the North Atlantic and the North Pacific.

194 2.4 Lagrangian Transport

195 We use Parcels (Probably A Really Computationally Efficient Lagrangian Simu-
 196 lator) (Lange & Van Sebille, 2017) to model microplastic as virtual particles which are
 197 advected using ocean flow field data. A change in the position \vec{x} of a particle is computed
 198 by:

$$199 \quad \vec{x}(t + \Delta t) = \vec{x}(t) + \int_t^{t+\Delta t} \vec{v}(\vec{x}(\tau), \tau) d\tau \quad (1)$$

200 where $\vec{v}(t)$ is the velocity at $\vec{x}(t)$. The flow velocity $\vec{v}(\vec{x}(t), t)$ at the particle location is
 201 obtained through linear interpolation of the flow field data in space and time.

202 All simulations are carried out for 2002-2014. Since the Geostrophic current dataset
 203 has a temporal resolution of 1 day, we use daily mean fields for the Total currents, Ek-
 204 man currents, Stokes drift and wind fields for consistency with the temporal resolution.
 205 We also carry out simulations with 3 hourly data to study the effect of current variations
 206 on sub-daily time scales.

207 For the initial microplastic distribution, we use a homogeneous distribution with
 208 particles placed at 1° intervals for the global simulations (34,515 particles). We also run
 209 separate simulations for the North Pacific and North Atlantic starting from a homoge-
 210 neous distribution with particles placed at 1/2° intervals (30,091 particles for the North
 211 Pacific and 18,632 particles for the North Atlantic), to allow better comparisons of the
 212 modeled distributions with observations. The majority of marine plastic debris is thought
 213 to enter the oceans from the coastlines from rivers (Lebreton et al., 2017), direct litter-
 214 ing at the coast (Jambeck et al., 2015) or as runoff from natural disasters (Prasetya, Black,
 215 De Lange, Borrero, & Healy, 2011). However, the input distribution remains highly un-
 216 certain (Lebreton et al., 2017). The input distribution is important for modeled concen-
 217 trations. However, since the purpose of this study is to determine the processes deter-
 218 mining the average spatial locations of the garbage patches, indicated by the spatial lo-
 219 cation of the peak microplastic concentration, it was assumed that the effect of the ini-
 220 tial distribution is small. This is supported for the long-term distribution by the close

agreement between the garbage patch locations modeled by Maximenko et al. (2012) (which started with particles with a initially homogeneous distribution) and those modeled by van Sebille et al. (2012) and Lebreton et al. (2012) (which released particles at the coasts scaled according to coastal population densities). The reported modeled concentrations are averaged over the final year of the 12-year simulation and binned into 1° bins to determine the average locations of the garbage patches.

The GlobCurrent datasets resolve some mesoscale eddies, and EKE is taken as a proxy for mesoscale eddy activity. Each particle samples the local EKE along its trajectory, where the EKE is computed from the Total surface current anomaly components u' and v' , which are computed with respect to the time-averaged Total surface currents for 2002-2014. The EKE is computed according to:

$$EKE = \frac{(u')^2 + (v')^2}{2}. \quad (2)$$

Preliminary simulations showed that almost half the particles beached over the course of a 12 year simulation. Since the purpose of this study does not involve investigating particle beaching, we implement an artificial shore-normal boundary current with a velocity of 1 m s^{-1} that is non-zero only at the coast. This prevented the beaching of particles and allowed for more robust statistics. The anti-beaching current is not found to influence the microplastic distribution.

3 Results

3.1 Global

Simulations with the Total currents show the formation of garbage patches in each of the subtropical ocean gyres, as well as north of Russia around Novaya Zemlya (Figure 2a), which agrees with observations (Cózar et al., 2014, 2017; Eriksen et al., 2014). The garbage patch with the most particles is in the South Pacific, but this is an artifact of the large number of particles within the basin at the beginning of the simulation, as was similarly stated by Maximenko et al. (2012). The garbage patches form as a result of the Ekman currents (Figure 2b), with the locations of the garbage patches matching those of the Total current garbage patches. The Ekman currents on their own lead to a smaller surface area of the garbage patch than with the Total currents, which is due to Geostrophic currents. The Geostrophic currents counter microplastic accumulation in the subtropics and disperse the microplastic over a larger surface area. On their own, the Geostrophic currents only lead to elevated concentrations in the open ocean north of Brazil and west of New Guinea (Figure 2c). However, this is likely a product of the Geostrophic current dataset, as the equatorial region has the highest estimated error of the Geostrophic currents relative to observations (Rio et al., 2016).

In the Pacific basins, Stokes drift largely clears the subtropical gyres of microplastic, transporting it east toward New Guinea (Figure 2d). Microplastic is found in the subtropical ocean gyre in the South Atlantic, but with low concentrations relative to garbage patch concentrations in the Total current simulation. Outside the equatorial regions, the highest concentrations are found near Antarctica and north of Norway, indicating that Stokes drift contributes to poleward microplastic transport.

The influence of Stokes drift is also apparent by comparing the connectivity of the ocean basins when particles are advected solely by Total currents or by the sum of Total currents and Stokes drift (Figure 3). Tracking the initially uniformly distributed particles indicate connections between the different ocean basins over a 12 year period, which show that the ocean basins do not follow strict cartographic boundaries. This is especially the case for the southern hemisphere (Figure 3a), where the basins stretch westwards in bands in the simulation with Total currents (Froyland, Stuart, & van Sebille,

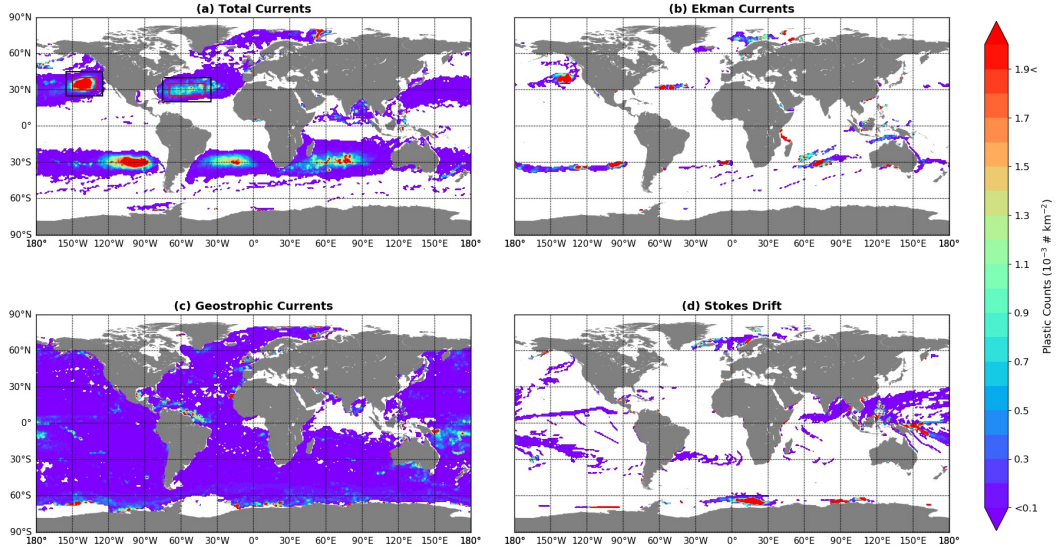


Figure 2. The average particle density of the final year of the global Lagrangian runs with the virtual particles advected by the daily mean Total, Ekman and Geostrophic currents and the Stokes drift. The red and black boxes in the North Pacific and North Atlantic in panel (a) indicate the garbage patch and extended garbage patch for that basin used in the EKE analysis.

269 2014). Only around half of all particles within the South Pacific, South Atlantic and Indian
 270 basins end within the same basin they originated from, compared to 96.0% and 82.0%
 271 for the North Pacific and North Atlantic (Table 2).

272 The inclusion of Stokes drift has a strong influence on these connections, particu-
 273 larly in the Southern Hemisphere (Figure 3b). The South Pacific has the greatest re-
 274 duction in particle number from 26.6% of the total particles to 15.8%, with the major-
 275 ity of these particles going either to the South Atlantic or the Indian basin. The increased
 276 connectivity with the North and South Pacific leads to a large increase in the number
 277 of particles in the Indian basin, which rises from 20.4% of the total particles to 27.4%
 278 (Table 2). This transport compensates for the increased connectivity between the South
 279 Atlantic and Indian basins, indicated by the share of particles in the South Atlantic that
 280 originate from the Indian basin rising from 28.2% to 39.6%.

281 The poleward transport due to Stokes drift, shown in Figure 2, is apparent by the
 282 213% increase in the total number of particles in the Southern basin at the end of the
 283 simulation relative to the simulation with just the Total currents. This increase is largely
 284 due to particles starting in the Southern basin being retained, although there are also
 285 increases in the number of particles reaching the Southern basin from the Indian, South
 286 Atlantic and South Pacific basins. There is also a slight increase of particles in the Ar-
 287 ctic basin due to increased poleward transport from the North Atlantic.

288 Finally, the inclusion of Stokes drift increases cross-equatorial particle transport.
 289 With just the Total currents, only 0.4% of particles in the South Atlantic originate from
 290 the North Pacific, while in the Indian basin the North Pacific share is 6.5%. This respec-
 291 tively rises to 3.3% and 19.2% with Stokes drift included. No particles from the North
 292 Atlantic are within the Southern Hemisphere at the end of the simulation.

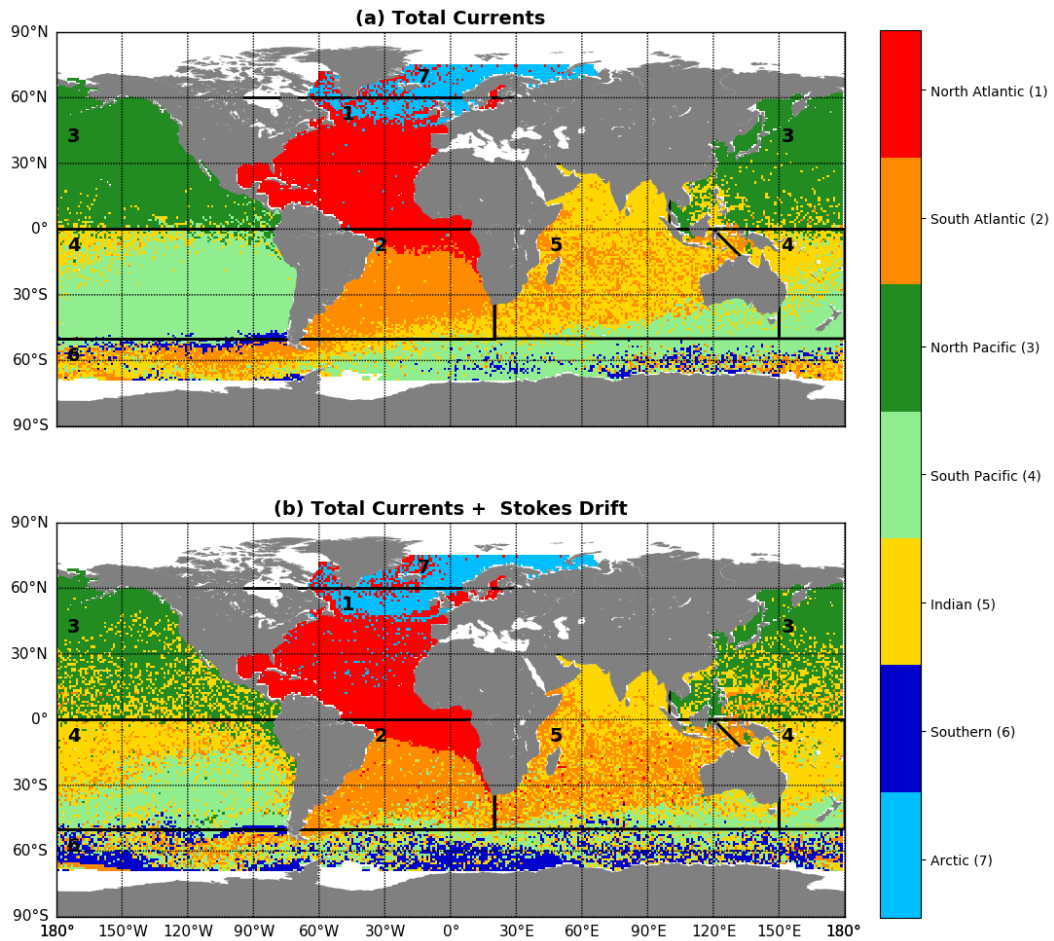


Figure 3. Connectivity of the ocean basins based on virtual particles advected with daily mean Total currents and the sum of the daily mean Total currents and Stokes drift. Particles are shown at their initial position colored according to their position at the end of the simulation. The coloring is based on the black boxes.

Table 2. The total number of particles within each basin (according to the definitions in Figure 3), at the end of the global simulations, with particles advected by either daily mean Total currents or the sum of the daily mean Total currents and Stokes drift. The left column indicates the basin of origin. Percentages indicate the fraction of total particles in the final basin that originate from the given basin of origin.

Basin of Origin	North Pacific		South Pacific		North Atlantic		South Atlantic	
	Total	Total + Stokes	Total	Total + Stokes	Total	Total + Stokes	Total	Total + Stokes
North Pacific	96.0%	93.4%	0.9%	0.0%	0.0%	0.0%	0.4%	3.3%
South Pacific	3.2%	5.1%	55.3%	46.6%	0.0%	0.0%	0.7%	9.2%
North Atlantic	0.0%	0.0%	0.0%	0.0%	82.0%	75.2%	0.0%	0.0%
South Atlantic	0.0%	0.1%	0.2%	3.5%	13.5%	17.2%	44.9%	34.3%
Indian	0.8%	1.0%	8.9%	12.6%	0.1%	2.0%	28.2%	39.6%
Southern	0.0%	0.4%	34.7%	37.3%	0.0%	0.4%	25.8%	13.6%
Arctic	0.0%	0.0%	0.0%	0.0%	4.4%	5.2%	0.0%	0.0%
Total Particles	7146	5809	9178	5452	4097	4205	4942	5603
Basin of Origin	Indian		Southern		Arctic			
	Total	Total + Stokes	Total	Total + Stokes	Total	Total + Stokes		
North Pacific	6.5%	19.2%	0.0%	0.0%	0.0%	0.0%		
South Pacific	18.1%	34.3%	5.0%	2.5%	0.0%	0.0%		
North Atlantic	0.0%	0.0%	0.0%	0.0%	38.8%	48.3%		
South Atlantic	5.3%	3.4%	0.0%	0.2%	0.7%	0.0%		
Indian	50.1%	28.6%	0.0%	1.8%	0.0%	0.0%		
Southern	20.0%	14.5%	95.0%	95.5%	0.0%	0.0%		
Arctic	0.0%	0.0%	0.0%	0.0%	60.5%	51.7%		
Total Particles	7028	9446	818	2557	1260	1405		

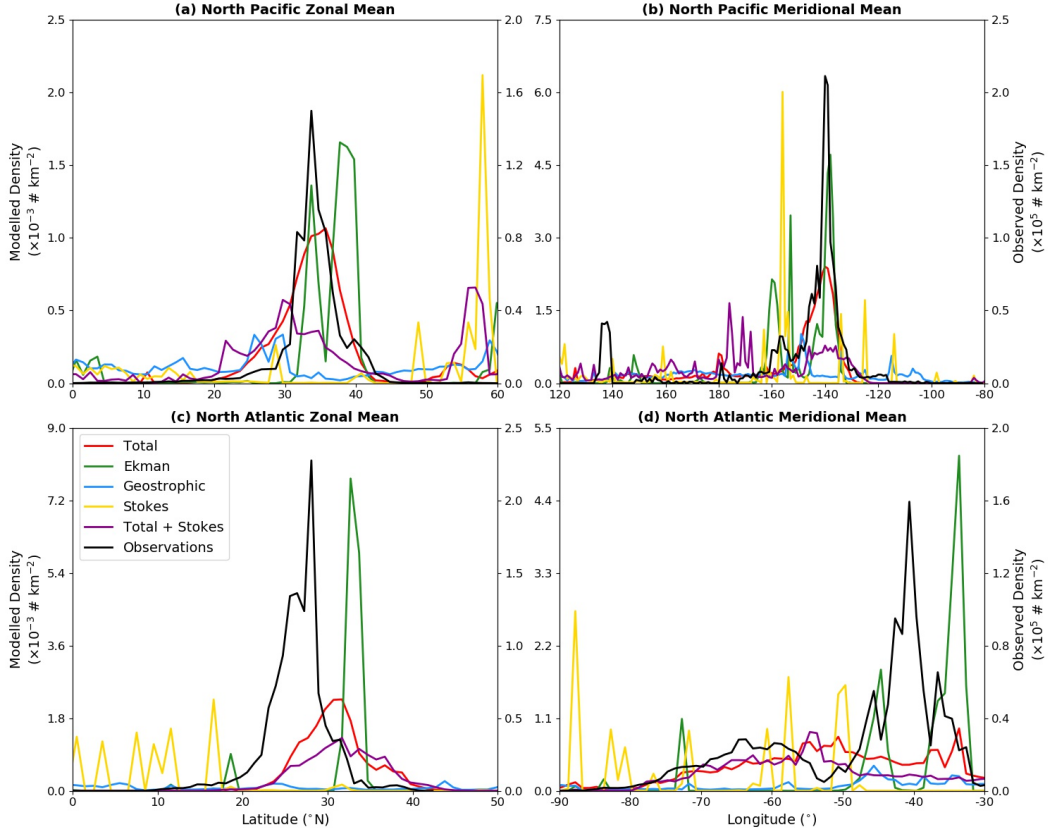


Figure 4. Zonal and meridional spatial means of observed (van Sebille et al., 2015) and modeled microplastic concentrations with various daily mean surface current components for the North Pacific and North Atlantic simulations. For the North Pacific the means are for the region of $0^{\circ} - 60^{\circ}\text{N}$ and $120^{\circ}\text{E} - 80^{\circ}\text{W}$. In the North Atlantic the means are for the region $0^{\circ} - 50^{\circ}\text{N}$ and $90^{\circ} - 30^{\circ}\text{W}$. In each subplot the left axis indicates the modeled concentrations while the right axis indicates the observed concentrations. Please note the different scales used in the subplots.

293

3.2 Comparison with Observations

294

We focus on the North Pacific and North Atlantic for the comparison of simulated distributions with observations as these are the only regions with a sufficient sampling density.

295

296

The North Pacific garbage patch with the Total currents shows good agreement with observations, with peaks in the meridional and zonal means of the microplastic concentration closely agreeing at $(35^{\circ}\text{N}, 140^{\circ}\text{W})$ (Figure 4a&b). In the North Atlantic the agreement is less clear. The model correctly predicts accumulation in the subtropics, but the highest concentrations are 5° farther north in the observations (Figure 4c). However, while the observational record has a pronounced peak in meridional mean microplastic concentration at 40°W , the elevated concentrations in the Total currents simulation are spread over $75^{\circ} - 30^{\circ}\text{W}$, with only small peaks at 34°W and $50^{\circ} - 55^{\circ}\text{W}$ (Figure 4d).

297

298

299

300

301

302

303

304

305

306

307

308

The zonal and meridional mean of the Geostrophic current simulation distribution show no elevated concentrations in the subtropics in neither the North Atlantic nor the North Pacific (Figure 4a&c). In contrast, the Ekman currents do lead to strong peaks in concentration in the subtropics, with the location of the concentration peaks in the

309 North Pacific closely agreeing with the concentration peaks in the observations (Figure
 310 4a&b). There is only a small shift in the position of the concentration peak relative to
 311 the concentration peak in the Total current distribution, indicating that Geostrophic cur-
 312 rents have little impact on the location of maximum accumulation. We do observe that
 313 the Ekman current simulations show much higher concentrations than the Total current
 314 simulations, which is due to the lack of strong dispersion of microplastic by the Geostrophic
 315 currents (Figure 2c).

316 In the North Atlantic the Ekman currents lead to the formation of two subtropi-
 317 cal microplastic concentration peaks at 35°W and 45°W (Figure 4d). These agree closely
 318 with the meridional concentration peak in the observations at 40°W. However, the ad-
 319 dition of Geostrophic currents spreads out the microplastic and the westernmost peak
 320 is found at 50° – 55°W. The location of easternmost peak is unaffected, but the con-
 321 centrations are lowered by a factor of five.

322 The addition of the drift to the Total currents does not lead to closer agreement
 323 between observed and modeled microplastic distributions (Figure 4). In the North Pa-
 324 cific the addition of Stokes drift causes much greater temporal variance in the location
 325 of the garbage patch, leading to a less defined garbage patch as the temporal averaging
 326 spreads out the peak concentrations over a larger area. The peak concentration in the
 327 zonal direction has shifted further south relative to observations, while there is no clear
 328 peak at all in the meridional direction (Figure 4a&b). In the North Atlantic the general
 329 shape of the microplastic distribution is unchanged in the zonal and meridional direc-
 330 tions, but the concentrations are consistently lower (Figure 4c&d).

331 **3.3 Role of Mesoscale Eddy Activity**

332 For the North Pacific and North Atlantic Total current simulations, time series of
 333 the average EKE are computed for all particles within the basins and for all particles
 334 whose final position at the end of the simulations are within the respective garbage patches.
 335 The garbage patches are selected such that they encompass the elevated microplastic con-
 336 centrations in the subtropical ocean gyre, as shown in Figure 2a. The extended garbage
 337 patches shift the garbage patch boundaries by 5° in each cardinal direction.

338 In the North Pacific the average EKE for particles in the garbage patch at the end
 339 of the simulation is consistently lower than the average for all particles (Figure 5a), which
 340 at the end of the simulation has grown by an order of magnitude. This is unchanged by
 341 considering the extended North Pacific patch. The time series of the extended garbage
 342 patch shows a similar trend, and indicates that observed trend is not just a product of
 343 the selected garbage patch boundaries.

344 The North Atlantic average EKE time series for all particles and just the garbage
 345 patch particles do not show a strong correlation (Pearson $r=0.560$, $p < 0.01$) and the av-
 346 erage EKE for the garbage patch particles is not consistently lower than the garbage patch
 347 as a whole (Figure 5b). There is a drop in the average EKE at the end of the simula-
 348 tion, but this is a product of the selected garbage patch boundaries as this drop is not
 349 visible when considering the extended North Atlantic garbage patch. There is therefore
 350 no indication that microplastic in the North Atlantic tends to accumulate in regions of
 351 relatively low mesoscale eddy activity.

352 **3.4 Comparison of Windage with Stokes Drift**

353 In the North Atlantic, particle advection in the two higher windage scenarios leads
 354 to particle distributions that are similar to the distribution from advection by Stokes drift
 355 in that particles are largely cleared from the subtropical open ocean in the higher windage
 356 scenarios (Figure 6). Furthermore we see most accumulation in the Carribbean or be-
 357 tween Greenland and Norway. However, with Stokes drift particles in the polar regions

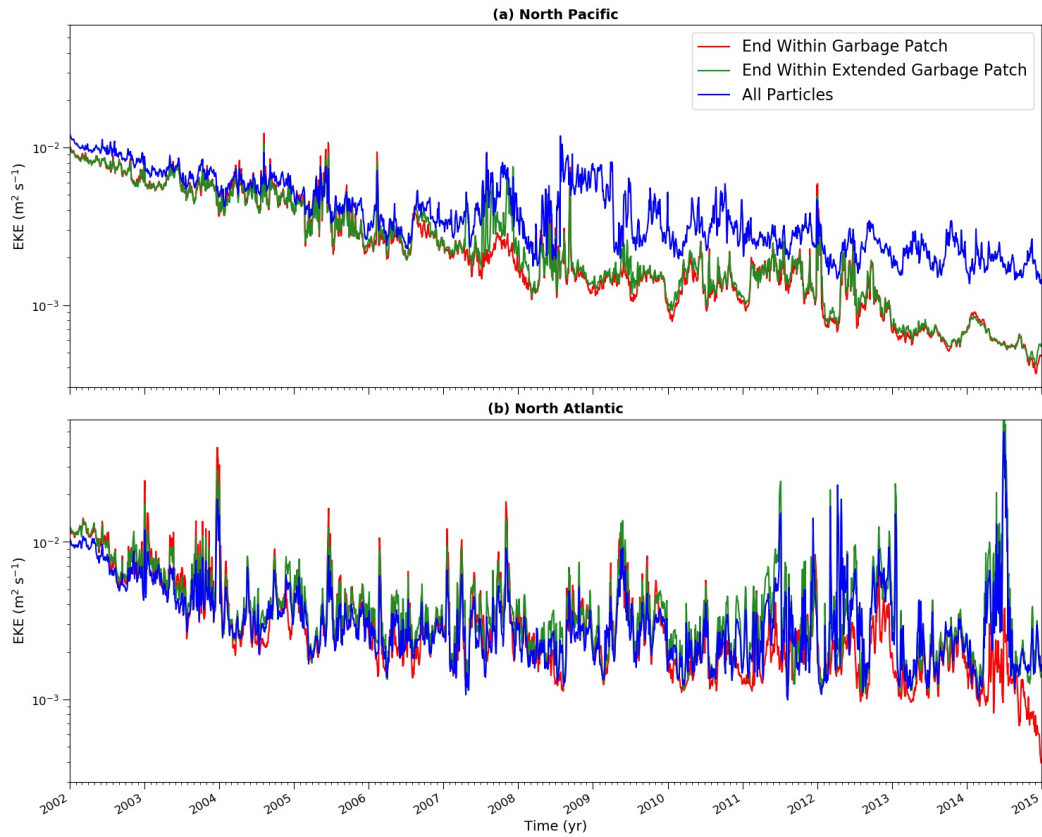


Figure 5. Average EKE over time of particles that end within the garbage patch, of particles that end within the extended garbage patch, and of all particles within the North Pacific and North Atlantic simulations. The particles are advected with daily mean Total currents. The North Atlantic garbage patch is defined as $25^{\circ} - 35^{\circ}\text{N}$ and $40^{\circ} - 70^{\circ}\text{W}$, while the extended North Atlantic garbage patch is defined as $20^{\circ} - 40^{\circ}\text{N}$ and $35^{\circ} - 75^{\circ}\text{W}$. The North Pacific garbage patch is defined as $30^{\circ} - 40^{\circ}\text{N}$ and $130^{\circ} - 150^{\circ}\text{W}$, while the extended North Pacific garbage patch is defined as $25^{\circ} - 45^{\circ}\text{N}$ and $125^{\circ} - 155^{\circ}\text{W}$, as shown in Figure 2a. Please note that the EKE axis is logarithmic.

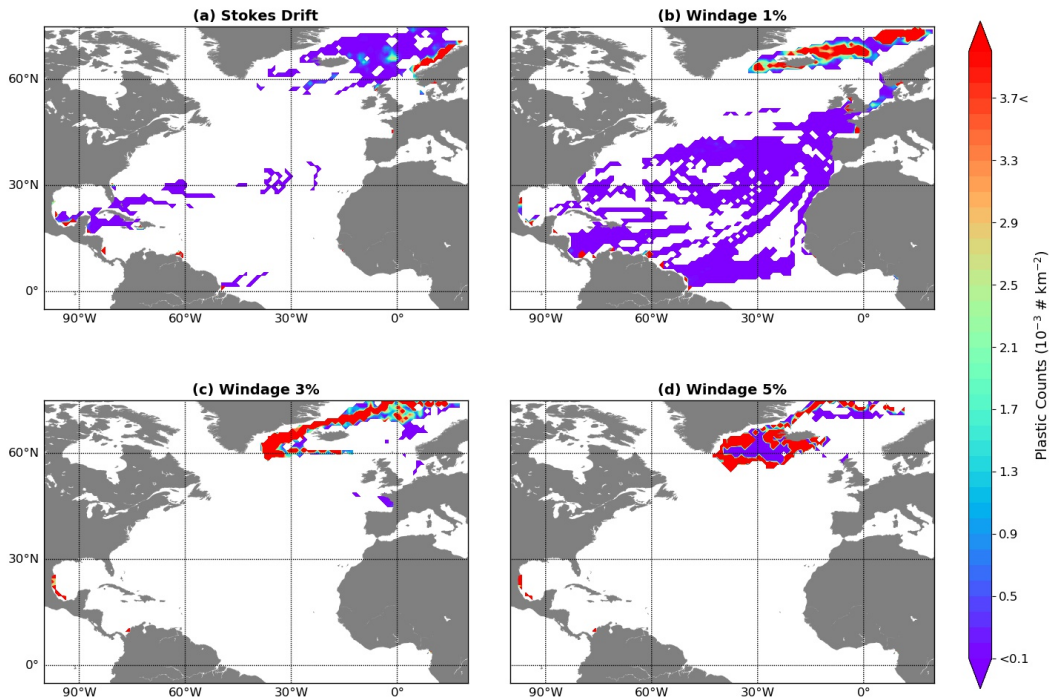


Figure 6. The average particle density of the final year of North Atlantic Lagrangian simulations with the virtual particles advected by daily mean Stokes drift and 1%, 3% and 5% windage from daily mean CFSR wind fields.

358 are largely driven towards the coast, while within the windage scenarios more particles
 359 tend to remain in the open ocean. Additionally, in the 1% windage scenario more particles
 360 remain in the subtropics than with Stokes drift. The high concentrations in the
 361 polar regions with each of the windage scenarios do not indicate a stable garbage patch,
 362 but are due to high numbers of particles passing through the region in the final simu-
 363 lation year.

364 All windage scenarios result in the same general microplastic distribution, but the
 365 3% and 5% windage scenarios result in particle velocities that are much higher than Stokes
 366 drift. The global average Root Mean Square Error (RMSE) of the 3% and 5% windage
 367 scenario Eulerian velocity fields relative to the Stokes drift Eulerian velocity fields are
 368 0.282 m s^{-1} and 0.225 m s^{-1} , while for the 1% windage scenario Eulerian velocity fields
 369 the global average RMSE is only 0.033 m s^{-1} . The RMSE is not globally uniform, with
 370 the smallest RMSE in the equatorial regions and the highest RMSE at $30^\circ - 60^\circ$ lati-
 371 tude and in the polar regions (Figure 7). The higher latitudes correspond to regions with
 372 a large amount of ocean swell, which have little correlation with local wind conditions
 373 (Fan, Lin, Griffies, & Hemer, 2014).

374 Considering the zonal and meridional velocity components of the Stokes drift and
 375 windage separately, there is a closer correlation between the zonal velocity components
 376 than the meridional components. With the zonal velocity, the coefficient of determina-
 377 tion (r^2) for most of the open ocean is 0.8 or higher, with lower coefficients only being
 378 found in the polar and select equatorial regions. In comparison, the coefficients of de-
 379 termination for the meridional velocity components are consistently lower. This has im-
 380 plications for the direction of the windage, for low correlation for either velocity com-
 381 ponent, results in the direction of the windage Eulerian velocity field deviating from the
 382 direction of the Stokes drift Eulerian velocity field.

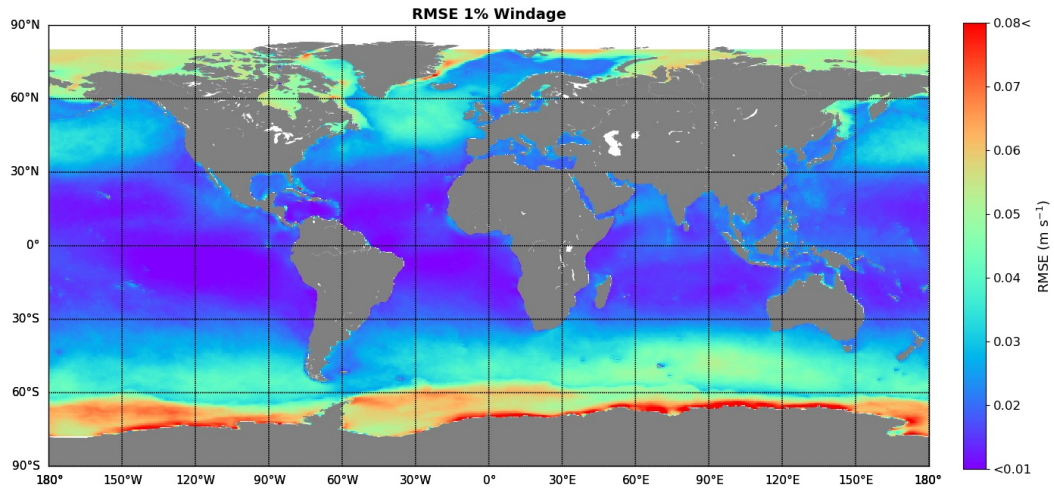


Figure 7. Root Mean Square Error (RMSE) between the speed of the Stokes drift and the 1% Windage scenario. The RMSE is computed on a $0.5^\circ \times 0.5^\circ$ grid for 01-01-2002 to 31-12-2014.

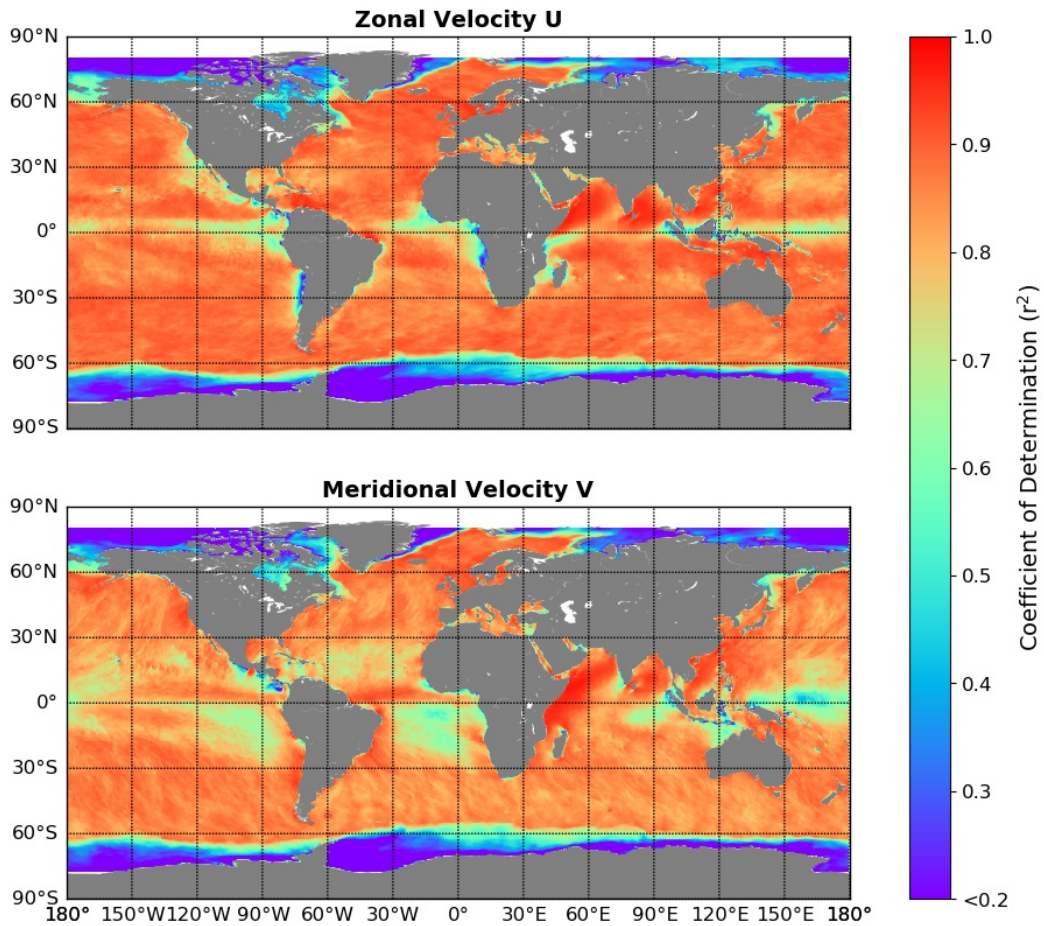


Figure 8. Coefficient of determination r^2 for the zonal and meridional velocity components of Stokes drift and windage. Coefficients are computed on a $0.5^\circ \times 0.5^\circ$ grid for 01-01-2002 to 31-12-2014.

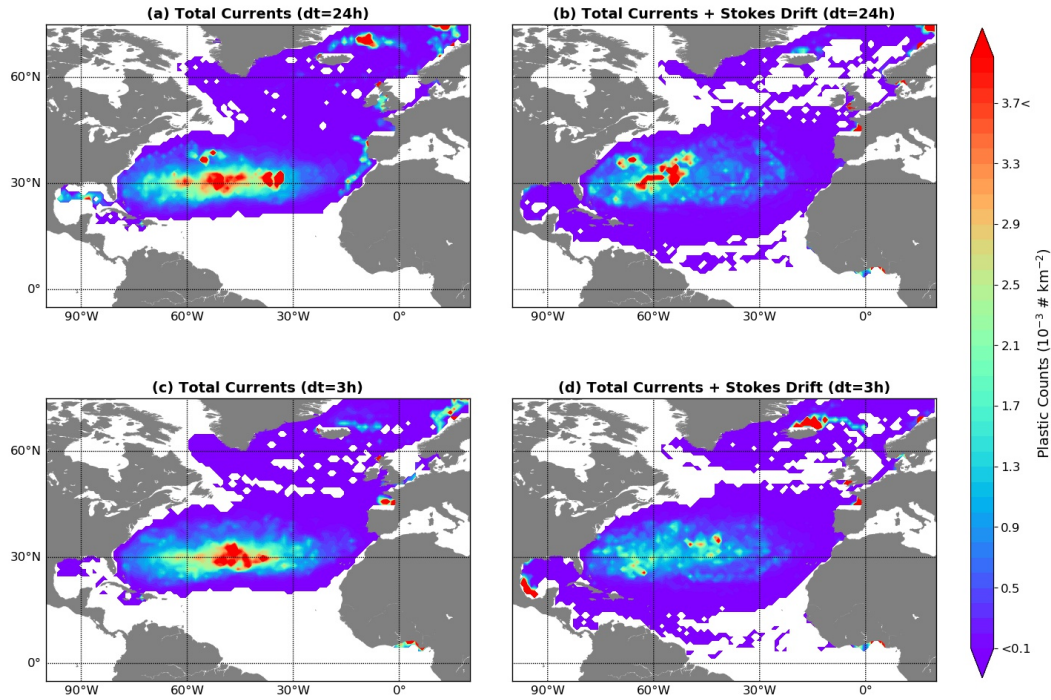


Figure 9. The average particle density of the final year of North Atlantic Lagrangian simulations with the virtual particles advected by Total currents or the sum of the Total currents and Stokes drift. The flow field datasets have a temporal resolution of either 24 hours or 3 hours.

383

3.5 Impact of Temporal Resolution of Flow Fields

384

385

386

387

388

389

390

Simulations of the North Atlantic where particles are advected using flow field datasets with a temporal resolution of 3 hours show that the higher temporal resolution of the Total currents does not have a strong impact on the modeled garbage patch (Figure 9a&c). The peak concentrations remain in the same location, although the zonal spread of microplastic is smaller when using the higher temporal resolution data set. In the case of the North Pacific the resultant microplastic distribution is similarly largely unaffected by the change in temporal resolution of the Total current dataset (Figure 10a&c).

391

392

393

394

395

396

397

398

399

The effect of the increased temporal resolution of the microplastic distribution is more apparent with the sum of the Total currents and Stokes drift. In the North Atlantic there is no clear peak in microplastic concentrations in the subtropics, as is the case when considering the daily mean flow field scenario (Figure 9b&d). There is also more microplastic in the Arctic regions, with high concentrations north of Iceland that are not visible with the lower temporal resolution. In the case of the North Pacific, the inclusion of Stokes drift with the daily mean datasets already results in there being no clear garbage patch in the subtropics, and increasing the temporal resolution does not change this (Figure 10b&d).

400

4 Discussion & Conclusions

401

402

403

404

In this study we investigate the role of various surface current components on the accumulation of microplastic in the subtropical ocean gyres. This is done by Lagrangian particle tracking with ocean circulation data from reanalysis products. The modeled microplastic distribution with the Total currents in the North Pacific, and to a lesser ex-

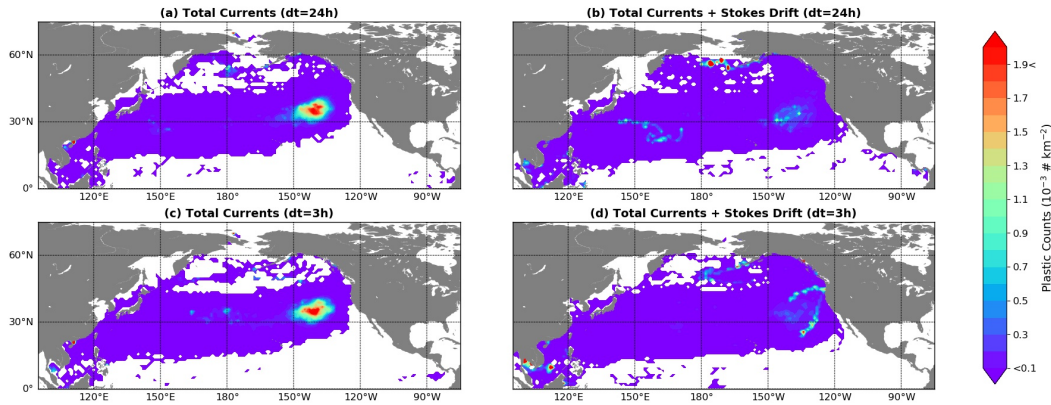


Figure 10. The average particle density of the final year of North Pacific Lagrangian simulations with the virtual particles advected by Total currents or the sum of the Total currents and Stokes drift. The flow field datasets have a temporal resolution of either 24 hours or 3 hours.

405 tent in the North Atlantic, show good agreement with the observational microplastic dis-
 406 tribution, and the location of the garbage patches is largely determined by the Ekman
 407 currents. This agrees with earlier work on the Pacific basins by Kubota (1994); Kubota
 408 et al. (2005) and Martinez et al. (2009), which found Ekman current to lead to debris
 409 transport to the subtropics, where Geostrophic currents transport the debris eastward.
 410 In our simulations we find the Ekman currents able to account for the eastward trans-
 411 port on their own. This is due to the angle of the surface Ekman currents to the surface
 412 wind stress being 30.75° instead of 45° as predicted by Ekman theory and used by Kub-
 413 ota (1994); Kubota et al. (2005) and Martinez et al. (2009). In the subtropics this leads
 414 to a stronger zonal velocity component and therefore more zonal microplastic transport.
 415 Considering the close agreement with observations, especially in the North Pacific, the
 416 GlobCurrent parametrization of the Ekman currents based on ARGO float Ekman ve-
 417 locities is likely a better indicator of the real surface ocean circulation than Ekman cur-
 418 rents computed solely based on Ekman theory.

419 Stokes drift has not been consistently considered in all global microplastic trans-
 420 port simulations, and this can lead to an underestimation of the microplastic contam-
 421 ination of polar regions. Our simulations showed that Stokes drift on its own does not
 422 contribute to microplastic accumulation in the subtropics, but we do observe high con-
 423 centrations near Antarctica and Norway. In contrast, the Total current simulations show
 424 very little microplastic near Antarctica. This is supported by Fraser et al. (2018), who
 425 found that Stokes drift can lead to help crossing the strong circumpolar winds and cur-
 426 rents to reach the Antarctic coast. Stokes drift therefore appears to be an important con-
 427 tributor to surface microplastic transport.

428 Unfortunately it is currently not possible to accurately determine the combined ef-
 429 fect of the Total and Stoke currents from reanalysis flow fields alone. The GlobCurrent
 430 and WaveWatch III datasets are not independent and the sum of Total currents and Stokes
 431 drift leads to overestimation of Stokes drift effects. The GlobCurrent surface Ekman cur-
 432 rents are parametrized based on the non-geostrophic velocities of ARGO drifters, and
 433 these drifter velocities contain a Stokes drift component (Rio et al., 2014). However, the
 434 parametrization of the Ekman currents is based on the local surface wind stress, and there-
 435 fore does not properly account for the contribution of ocean swell to Stokes drift. This
 436 is shown by our comparison of Stokes drift with the windage scenarios, where regions
 437 with high amounts of ocean swell show a higher RMSE between the Eulerian velocity
 438 fields of Stokes drift and the 1% windage scenario. We also see that the windage direc-

439 tion does not always agree with the direction of Stokes drift, which can have important
440 implications for transport modeling. This is especially the case for polar regions, which
441 are most affected by transport due to Stokes drift but where we also see the greatest dis-
442 crepancy between Stokes drift and windage scenarios.

443 There is a need for instruments capable of direct global measurements of Stokes
444 drift in the open ocean. This would provide a global observation dataset of Stokes drift,
445 which in turn can be used to correct for Stokes drift in the parametrization of Ekman
446 currents. In this manner, summation of all current components would be possible and
447 further analysis of the contribution of Stokes drift to microplastic transport would be
448 possible. The recently proposed SKIM satellite would use near-nadir Ka-band Doppler
449 radar with incidence angles of 6° and 12° to measure the directional wave spectrum, from
450 which the Stokes drift can be derived (Ardhuin et al., 2018). The measured velocity fields
451 would have a temporal resolution of 1 hour, which would be of great use for Stokes drift,
452 since Stokes drift transport appears more sensitive to the temporal resolution of the datasets
453 than the transport due to Ekman and Geostrophic currents. This is due to Stokes drift
454 being dependent on the wave field, which responds quickly to changes in atmospheric
455 conditions. In contrast, geostrophic balance responds to changes in conditions on timescales
456 of days.

457 Martinez et al. (2009) first found that marine debris tends to accumulate in regions
458 of low EKE, and for the North Pacific we verify similar behavior. Maes et al. (2016) showed
459 the inclusion of mesoscale eddies results in more debris escaping the North Pacific garbage
460 patch. Since mesoscale eddies can transport mass, our initial hypothesis was that higher
461 microplastic concentrations are observed in regions of low EKE since these are regions
462 where there is less mesoscale eddy activity. In regions of low mesoscale eddy activity, this
463 would happen less frequently and therefore high concentrations can be maintained. In
464 the North Pacific the region of low EKE coincides with the subtropical ocean gyre, and
465 so Ekman currents can transport microplastic to the garbage patch. The low EKE can
466 contribute to the maintenance of the elevated concentrations, since low mesoscale eddy
467 activity would indicate that less eddies are present within the region to carry away mi-
468 croplastic. In the North Pacific this hypothesis remains plausible, but we would expect
469 to see similar patterns in the North Atlantic. Theoretical work has suggested that the
470 EKE of subtropical gyres scales with the basin size (Spall, 2000), and therefore it is pos-
471 sible that the smaller size of the North Atlantic basin leads to a less prominent role for
472 mesoscale eddy activity. On the other hand, we see that the modeled North Atlantic garbage
473 patch has a larger zonal extent than in the North Atlantic. This might be due to an ab-
474 sence of a local minimum in the EKE, with microplastic dispersion due to mesoscale eddy
475 activity being constant throughout the subtropics. However, these remain hypotheses.

476 While we model transport as being purely two dimensional, biofouling of microplas-
477 tic particles results in decreased buoyancy, which leads to sinking Kooi, van Nes, Schef-
478 fer, and Koelmans (2017). Additionally, we do not consider microplastic removal pro-
479 cesses, such as beaching and ingestion. Therefore, future microplastic modeling might
480 consider three dimensional flow fields with vertical microplastic dynamics and account
481 for microplastic removal. Furthermore, in this paper we only compare our modeled dis-
482 tributions with observations in the North Pacific and North Atlantic due to insufficient
483 sampling of the other ocean basins. There is therefore a great need for more microplas-
484 tic sampling, especially outside the eastern North Pacific and the Western North Atlantic.

485 Acknowledgments

486 The code used for this work is distributed under the MIT license and can be found at
487 <https://github.com/OceanParcels/SKIM-garbagepatchlocations>. The v3.0 GlobCurrent
488 data can be found at <http://www.ifremer.fr/opendap/cerdap1/globcurrent/v3.0/> and
489 the WaveWatch III hindcast can be found at <ftp://ftp.ifremer.fr/ifremer/ww3/HINDCAST/GLOBAL/>.

490 This work was funded by the European Space Agency (ESA) through the Sea sur-
 491 face KInematics Multiscale monitoring (SKIM) Mission Science (SciSoc) Study (Con-
 492 tract 4000124734/18/NL/CT/gp). Erik van Sebille was supported through funding from
 493 the European Research Council (ERC) under the European Union’s Horizon 2020 re-
 494 search and innovation programme (grant agreement No 715386).

495 References

- 496 Ardhuin, F., Aksenov, Y., Benetazzo, A., Bertino, L., Brandt, P., Caubet, E., . . .
 497 Xie, J. (2018). Measuring currents, ice drift, and waves from space: the sea
 498 surface kinematics multiscale monitoring (skim) concept. *Ocean Science*,
 499 *14*(3), 337–354.
- 500 Bennett, V. C., & Mulligan, R. P. (2017). Evaluation of surface wind fields for pre-
 501 diction of directional ocean wave spectra during hurricane sandy. *Coastal Engi-
 502 neering*, *125*, 1–15.
- 503 Brach, L., Deixonne, P., Bernard, M. F., Durand, E., Desjean, M. C., Perez, E., . . .
 504 ter Halle, A. (2018). Anticyclonic eddies increase accumulation of microplastic
 505 in the north atlantic subtropical gyre. *Marine Pollution Bulletin*, *126*, 191–96.
- 506 Breivik, Ø., & Allen, A. A. (2008). An operational search and rescue model for the
 507 norwegian sea and the north sea. *Journal of Marine Systems*, *69*(1-2), 99–113.
- 508 Chubarenko, I., Bagaev, A., Zobkov, M., & Esiukova, E. (2016). On some physical
 509 and dynamical properties of microplastic particles in marine environment. *Ma-
 510 rine pollution bulletin*, *108*(1-2), 105–112.
- 511 Cózar, A., Echevarria, F., González-Gordillo, J. I., Irigoien, X., Ubeda, B.,
 512 Hernandez-Leon, S., . . . Duarte, C. M. (2014). Plastic debris in the open
 513 ocean. *Proceedings of the National Academy of Sciences*, *111*(28), 10239-
 514 10244.
- 515 Cózar, A., Martí, E., Duarte, C. M., García-De-Lomas, J., Sebille, E. V., Ballatore,
 516 T. J., . . . Irigoien, X. (2017). The arctic ocean as a dead end for floating
 517 plastics in the north atlantic branch of the thermohaline circulation. *Science
 518 Advances*, *3*(4), 1-8.
- 519 Dee, D. P., Uppala, S. M., Simmons, A. J., Berrisford, P., Poli, P., Kobayashi, S., . . .
 520 Vitart, F. (2011). The era-interim reanalysis: Configuration and performance
 521 of the data assimilation system. *Quarterly Journal of the Royal Meteorological
 522 Society*, *137*(656), 553–597.
- 523 Drivdal, M., Broström, G., & Christensen, K. (2014). Wave-induced mixing and
 524 transport of buoyant particles: application to the statfjord a oil spill. *Ocean
 525 Science*, *10*(6), 977–991.
- 526 Duhec, A. V., Jeanne, R. F., Maximenko, N., & Hafner, J. (2015). Composition
 527 and potential origin of marine debris stranded in the western indian ocean on
 528 remote alphonse island, seychelles. *Marine pollution bulletin*, *96*(1-2), 76–86.
- 529 Eden, C., & Böning, C. (2002). Sources of eddy kinetic energy in the labrador sea.
 530 *Journal of Physical Oceanography*, *32*(12), 3346–3363.
- 531 Eriksen, M., Lebreton, L. C. M., Carson, H. S., Thiel, M., Moore, C. J., Borrorro,
 532 J. C., . . . Reisser, J. (2014). Plastic pollution in the world’s oceans: More than
 533 5 trillion plastic pieces weighing over 250,000 tons afloat at sea. *PLoS ONE*,
 534 *9*(12), 1-15.
- 535 Eriksen, M., Maximenko, N., Thiel, M., Cummins, A., Lattin, G., Wilson, S., . . .
 536 Rifman, S. (2013). Plastic pollution in the south pacific subtropical gyre.
 537 *Marine Pollution Bulletin*, *68*(1-2), 71–76.
- 538 Fan, Y., Lin, S.-J., Griffies, S. M., & Hemer, M. A. (2014). Simulated global swell
 539 and wind-sea climate and their responses to anthropogenic climate change at
 540 the end of the twenty-first century. *Journal of Climate*, *27*(10), 3516–3536.
- 541 Fraser, C. I., Morrison, A. K., Hogg, A. M., Macaya, E. C., van Sebille, E., Ryan,
 542 P. G., . . . Waters, J. M. (2018, Jul). Antarcicas ecological isolation will be

- 543 broken by storm-driven dispersal and warming. *Nature Climate Change*. doi:
 544 10.1038/s41558-018-0209-7
- 545 Froyland, G., Stuart, R. M., & van Sebille, E. (2014). How well-connected is the sur-
 546 face of the global ocean? *Chaos*, *24*, 3.
- 547 Galgani, F., Leaute, J., Moguedet, P., Souplet, A., Verin, Y., Carpentier, A., ...
 548 others (2000). Litter on the sea floor along european coasts. *Marine pollution*
 549 *bulletin*, *40*(6), 516–527.
- 550 Henderson, J. R. (2001). A pre-and post-marpol annex v summary of hawaiian
 551 monk seal entanglements and marine debris accumulation in the northwestern
 552 hawaiian islands, 1982–1998. *Marine Pollution Bulletin*, *42*(7), 584–589.
- 553 Jambeck, J. R., Geyer, R., Wilcox, C., Siegler, T. R., Perryman, M., Andrady, A.,
 554 ... Law, K. L. (2015). Plastic waste inputs from land into the ocean. *Science*,
 555 *347*(6223), 768–771.
- 556 Kooi, M., van Nes, E. H., Scheffer, M., & Koelmans, A. A. (2017). Ups and downs
 557 in the ocean: effects of biofouling on vertical transport of microplastics. *Envi-*
 558 *ronmental Science & Technology*, *51*(14), 7963–7971.
- 559 Kubota, M. (1994). A mechanism for the accumulation of floating marine debris
 560 north of hawaii. *Journal of Physical Oceanography*, *24*(5), 1059–1064.
- 561 Kubota, M., Takayama, K., & Namimoto, D. (2005). Pleading for the use of
 562 biodegradable polymers in favor of marine environments and to avoid an
 563 asbestos-like problem for the future. *Applied Microbiology and Biotechnology*,
 564 *67*(4), 469–476.
- 565 Kukulka, T., Proskurowski, G., Morét-Ferguson, S., Meyer, D. W., & Law, K. L.
 566 (2012). The effect of wind mixing on the vertical distribution of buoyant
 567 plastic debris. *Geophysical Research Letters*, *39*(7), 1–6.
- 568 Lange, M., & Van Sebille, E. (2017). Parcels v0.9: Prototyping a lagrangian ocean
 569 analysis framework for the petascale age. *Geoscientific Model Development Dis-*
 570 *cussions*, *10*, 4175–4186.
- 571 Law, K. L., Moret-Ferguson, S., Maximenko, N. A., Proskurowski, G., Peacock,
 572 E. E., Hafner, J., & Reddy, C. M. (2010). Plastic accumulation in the north
 573 atlantic subtropical gyre. *Science*, *329*(5996), 1185–1188.
- 574 Law, K. L., Moret-Ferguson, S. E., Goodwin, D. S., Zettler, E. R., Deforce, E.,
 575 Kukulka, T., & Proskurowski, G. (2014). Distribution of surface plastic debris
 576 in the eastern pacific ocean from an 11-year data set. *Environmental Science &*
 577 *Technology*, *48*(9), 4732–4738.
- 578 Lebreton, L.-M., Greer, S., & Borrero, J. (2012). Numerical modelling of floating de-
 579 bris in the world’s oceans. *Marine Pollution Bulletin*, *64*(3), 653–661.
- 580 Lebreton, L.-M., Slat, B., Ferrari, F., Sainte-Rose, B., Aitken, J., Marthouse, R., ...
 581 Reisser, J. (2018). Evidence that the great pacific garbage patch is rapidly
 582 accumulating plastic. *Scientific Reports*, *8*(1).
- 583 Lebreton, L.-M., Van Der Zwet, J., Damsteeg, J.-W., Slat, B., Andrady, A., &
 584 Reisser, J. (2017). River plastic emissions to the world’s oceans. *Nature*
 585 *Communications*, *8*, 15611.
- 586 Maes, C., Blanke, B., & Martinez, E. (2016). Origin and fate of surface drift in the
 587 oceanic convergence zones of the eastern pacific. *Geophysical Research Letters*,
 588 *43*(7), 3398–3405.
- 589 Martinez, E., Maamaatuaiahutapu, K., & Taillandier, V. (2009). Floating marine
 590 debris surface drift: Convergence and accumulation toward the south pacific
 591 subtropical gyre. *Marine Pollution Bulletin*, *58*(9), 1347–1355.
- 592 Mascarenhas, R., Santos, R., & Zeppelini, D. (2004). Plastic debris ingestion by sea
 593 turtle in paraiba, brazil. *Marine pollution bulletin*, *49*(4), 354–355.
- 594 Maximenko, N., Hafner, J., & Niiler, P. (2012). Pathways of marine debris derived
 595 from trajectories of lagrangian drifters. *Marine Pollution Bulletin*, *65*(1-3), 51-
 596 62.
- 597 Molnar, J. L., Gamboa, R. L., Revenga, C., & Spalding, M. D. (2008). Assessing

- 598 the global threat of invasive species to marine biodiversity. *Frontiers in Ecol-*
599 *ogy and the Environment*, 6(9), 485–492.
- 600 Montiel, F., Squire, V., Doble, M., Thomson, J., & Wadhams, P. (2018). Atten-
601 uation and directional spreading of ocean waves during a storm event in the
602 autumn beaufort sea marginal ice zone. *Journal of Geophysical Research:*
603 *Oceans*.
- 604 Morét-Ferguson, S., Law, K. L., Proskurowski, G., Murphy, E. K., Peacock, E. E., &
605 Reddy, C. M. (2010). The size, mass, and composition of plastic debris in the
606 western north atlantic ocean. *Marine Pollution Bulletin*, 60(10), 1873–1878.
- 607 Pieper, C., Ventura, M. A., Martins, A., & Cunha, R. T. (2015). Beach debris in
608 the azores (ne atlantic): Faial island as a first case study. *Marine pollution bul-*
609 *letin*, 101(2), 575–582.
- 610 Prasetya, G., Black, K., De Lange, W., Borrero, J., & Healy, T. (2011). Debris
611 dispersal modeling for the great sumatra tsunamis on banda aceh and sur-
612 rounding waters. *Natural Hazards*, 60(3), 1167-188.
- 613 Rio, M.-H., Johannessen, J., & Donlan, C. (2016). *Product data handbook: The com-*
614 *combined geostrophy+ekman currents* (Tech. Rep.). Globcurrent.
- 615 Rio, M.-H., Mulet, S., & Picot, N. (2014). Beyond goce for the ocean circulation es-
616 timate: Synergetic use of altimetry, gravimetry, and in situ data provides new
617 insight into geostrophic and ekman currents. *Geophysical Research Letters*,
618 41(24), 8918-925.
- 619 Saha, S., Moorthi, S., Wu, X., Wang, J., Nadiga, S., Tripp, P., ... others (2011).
620 Ncep climate forecast system version 2 (cfsv2) 6-hourly products. *Research*
621 *Data Archive at the National Center for Atmospheric Research, Computational*
622 *and Information Systems Laboratory*.
- 623 Spall, M. A. (2000). Generation of strong mesoscale eddies by weak ocean gyres.
624 *Journal of marine research*, 58(1), 97–116.
- 625 Thompson, R. C., Olsen, Y., Mitchell, R. P., Davis, A., Rowland, S. J., John,
626 A. W. G., ... Russell, A. E. (2004). Lost at sea: Where is all the plastic?
627 *Science*, 304(5672), 838.
- 628 Tolman, H. L. (1997). *User manual and system documentation of wavewatch-iii ver-*
629 *sion 1.15*. US Department of Commerce, National Oceanic and Atmospheric
630 Administration, National Weather Service, National Centers for Environmental
631 Prediction.
- 632 Tolman, H. L. (2009). User manual and system documentation of wavewatch iii tm
633 version 3.14. *Technical note, MMAB Contribution*, 276, 220.
- 634 Trinanes, J. A., Olascoaga, J. M., Goni, G. J., Maximenko, N. A., Griffin, D. A.,
635 & Hafner, J. (2016). Analysis of flight mh370 potential debris trajectories
636 using ocean observations and numerical model results. *Journal of Operational*
637 *Oceanography*, 9(2), 126-138.
- 638 van Sebille, E., England, M. H., & Froyland, G. (2012). Origin, dynamics and evo-
639 lution of ocean garbage patches from observed surface drifters. *Environmental*
640 *Research Letters*, 7(4), 1-6.
- 641 van Sebille, E., Wilcox, C., Lebreton, L., Maximenko, N., Hardesty, B. D., Van
642 Franeker, J. A., ... Law, K. L. (2015). A global inventory of small floating
643 plastic debris. *Environmental Research Letters*, 10(12), 1-11.
- 644 Van Cauwenberghe, L., Vanreusel, A., Mees, J., & Janssen, C. R. (2013). Microplas-
645 tic pollution in deep-sea sediments. *Environmental Pollution*, 182, 495–499.
- 646 van den Bremer, T., & Breivik, Ø. (2018). Stokes drift. *Phil. Trans. R. Soc. A*,
647 376(2111), 20170104.
- 648 van Franeker, J. A., & Law, K. L. (2015). Seabirds, gyres and global trends in plas-
649 tic pollution. *Environmental Pollution*, 203, 89–96.
- 650 Webb, A., & Fox-Kemper, B. (2015). Impacts of wave spreading and multidirec-
651 tional waves on estimating stokes drift. *Ocean Modelling*, 96, 49-64.
- 652 Young, A. M., & Elliott, J. A. (2016). Characterization of microplastic and meso-

653 plastic debris in sediments from kamilo beach and kahuku beach, hawai'i. *Ma-*
654 *rine pollution bulletin*, 113(1-2), 477-482.